

Electromagnetic calorimeters based on scintillating lead tungstate crystals for experiments at Jefferson Lab [☆]

A.Asaturyan^a, F.Barbosa^c, V.Berdnikov^b, E.Chudakov^c, J.Crafts^{b,c}, H.Egiyan^c,
L.Gan^f, A.Gasparian^g, K.Harding^c, T.Horn^b, V.Kakoyan^a, H.Mkrtchyan^a,
Z.Papandreou^e, V. Popov^c, N.Sandoval^c, A.Somov^{c,*}, S.Somov^d, A. Smith^h, C.
Stanislav^c, S.Taylor^c, H. Voskanyan^a, T. Whitlatch^c, S. Worthington^c

^aA. I. Alikhanian National Science Laboratory (Yerevan Physics Institute), 0036 Yerevan, Armenia

^bThe Catholic University of America, Washington, DC 20064, USA

^cThomas Jefferson National Accelerator Facility, Newport News, VA 23606, USA

^dNational Research Nuclear University MEPhI, Moscow 115409, Russia

^eUniversity of Regina, Regina, Saskatchewan, Canada S4S 0A2

^fUniversity of North Carolina at Wilmington, Wilmington, NC 28403, USA

^gNorth Carolina A&T State University, Greensboro, NC 27411, USA

^hDuke University, Durham, NC 27708, USA

Abstract

A new electromagnetic calorimeter consisting of 140 lead tungstate (PbWO₄) scintillating crystals was constructed for the PrimEx- η experiment at Jefferson lab. The calorimeter was integrated into the data acquisition and trigger systems of the GlueX detector and used in the experiment to reconstruct Compton scattering events. The experiment started collecting data in the spring of 2019 and acquired about 30% of the required statistics. The calorimeter is a prototype for two PbWO₄-based detectors: the Neutral Particle Spectrometer (NPS) and the lead tungstate insert of the forward calorimeter (FCAL) of the GlueX detector. The article presents the design and performance of the Compton calorimeter and gives a brief overview of the FCAL and NPS projects.

Keywords: Electromagnetic calorimeter, Lead tungstate scintillator

[☆]Notice: Authored by Jefferson Science Associates, LLC under U.S. DOE Contract No. DE-AC05-06OR23177. The U.S. Government retains a non-exclusive, paid-up, irrevocable, world-wide license to publish or reproduce this manuscript for U.S. Government purposes.

*Corresponding author. Tel.: +1 757 269 5553; fax: +1 757 269 6331.

Email address: somov@jlab.org (A.Somov)

1. Introduction

Electromagnetic calorimeters based on PbWO_4 scintillating crystals have a widespread application in experiments at different accelerator facilities such as CERN, FNAL, GSI, and Jefferson Lab (JLab). The small radiation length ($L_R = 0.89$ cm) and Molière radius ($R_M = 2.19$ cm) of PbWO_4 allows to build high-granularity detectors with a good spatial separation and energy resolution of reconstructed electromagnetic showers, which makes these crystals the material of choice in many of these applications.

Two electromagnetic calorimeters are currently under construction in experimental Hall D and Hall C at Jefferson Lab, both using rectangular 2.05 cm \times 2.05 cm \times 20 cm PbWO_4 scintillating modules. The inner part of the forward lead glass calorimeter of the GlueX detector [1] in Hall D will be upgraded with these high-granularity, high-resolution crystals. This upgrade is required by the JLab Eta Factory (JEF) experiment to perform precision measurements of various $\eta^{(\prime)}$ decays with emphasis on rare neutral modes [2]. The Neutral Particle Spectrometer [3] in experimental Hall C consists of a PbWO_4 electromagnetic calorimeter preceded by a sweeping magnet. The NPS is required by Hall C's precision cross section measurement program with neutral final states [4–9]. Such precision measurements of small cross sections play a central role in studies of transverse spatial and momentum hadron structure. The NPS detector consists of 1080 PbWO_4 crystals arranged in a 30×36 array. Lead tungstate crystals for both detectors were procured from two vendors: Shanghai Institute of Ceramics (SICCAS) in China and CRYTUR in the Czech Republic. The quality of recently produced PbWO_4 scintillators has been studied in detail by the NPS and EIC eRD1 collaborations and is described in Ref. [10]. PbWO_4 crystals are also being considered for an electromagnetic calorimeter of the future Electron-Ion Collider [11].

In this article we describe the design and construction of a calorimeter prototype composed of 140 SICCAS crystals, which served as the Compton Calorimeter (CCAL) in the PrimEx- η experiment [12] with the GlueX detector in the spring of 2019. The CCAL was subsequently used during a few short GlueX physics runs at high luminosity in order to study rates and operating conditions expected for the FCAL lead-tungstate insert. Experience gained during fabrication and operation of the CCAL was critical

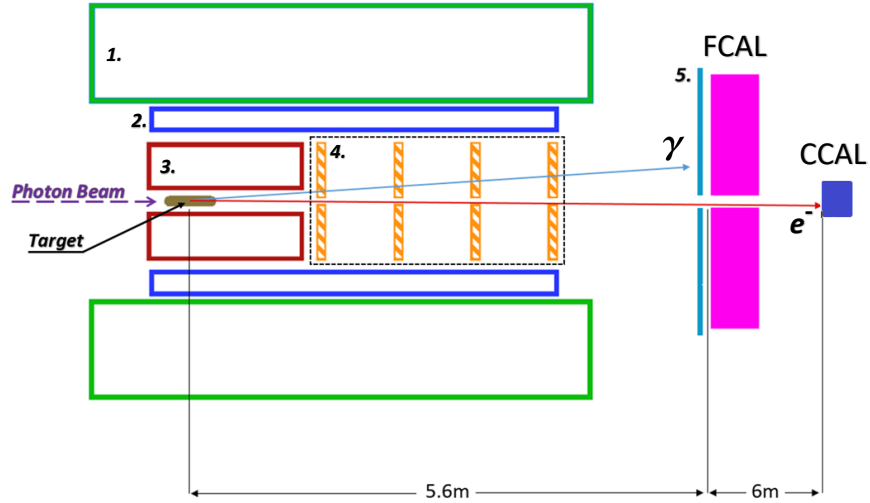


Figure 1: Schematic layout of the GlueX detector (not to scale). Numbers represent the following detector components: solenoid magnet (1), barrel calorimeter (2), central drift chamber (3), forward drift chambers (4), time-of-flight wall (5).

31 for finalizing the design of the FCAL insert and also helped further optimize the NPS
 32 calorimeter.

33 This article is organized as follows: we will present the PrimEx- η experiment and
 34 performance of the CCAL in Section 2 and Section 3, and will briefly describe the
 35 FCAL and NPS projects in Sections 4 and 5.

36 2. PrimEx- η experiment with the GlueX detector

37 The GlueX detector [1] was designed to perform experiments using a photon beam.
 38 Beam photons are produced via the bremsstrahlung process by electrons, provided by
 39 the JLab electron accelerator facility, incident on a thin radiator. The energy of a beam
 40 photon (E_γ) is determined by detecting a scattered electron after radiating the photon

41 as follows: $E_\gamma = E_e - E'_e$, where E_e is the primary electron beam energy and E'_e is
42 the energy of the bremsstrahlung electron. The bremsstrahlung electron is deflected
43 in a 6 m long dipole magnet operated at a field of ~ 1.5 T and registered in the so-
44 called tagging scintillator counters. Each counter corresponds to the specific energy
45 of the reconstructed lepton. The tagging detectors span the beam photon energy range
46 between 25% and 98% of the electron beam energy and covered the range between 2.8
47 GeV and 11.0 GeV during the PrimEx- η experiment¹. The typical energy resolution of
48 the beam photon is about 0.1%. The photon beam propagates toward the GlueX target.
49 A schematic view of the GlueX detector is illustrated in Fig. 1².

50 The physics goal of the PrimEx- η experiment is to perform a precision measure-
51 ment of the $\eta \rightarrow \gamma\gamma$ decay width. The measurement will provide an important test
52 of quantum chromodynamics symmetries and is essential for the determination of fun-
53 damental properties such as the ratios of the light quark masses and the η - η' mixing
54 angle. The decay width will be extracted from the measurement of the photoproduc-
55 tion cross section of η mesons in the Coulomb field of a nucleus, which is known as the
56 Primakoff effect. The η mesons will be reconstructed by detecting two decay photons
57 in the forward calorimeter of the GlueX detector.

58 The cross section will be normalized using the Compton scattering process, which
59 will also be used to monitor the luminosity and control the detector stability during
60 data taking. Electrons and photons originating from Compton events in the target are
61 produced at small angles, typically outside the acceptance of the FCAL. In order to im-
62 prove the reconstruction of particles in the forward direction, we built a small Compton
63 calorimeter consisting of 140 lead tungstate scintillating crystals and positioned it about
64 6 m downstream from the FCAL as shown in Fig. 1. The CCAL covers the angular
65 range between 0.19° and 0.47° .

66 The PrimEx- η experiment started collecting data in the spring of 2019 and has
67 acquired 30% of the required statistics. During the experiment, the magnetic field

¹The electron beam energy during most production PrimEx- η runs was 11.2 GeV.

²Not shown on this plot is the DIRC detector, which was installed after the PrimEx- η experiment and is used for the particle identification in the forward direction.

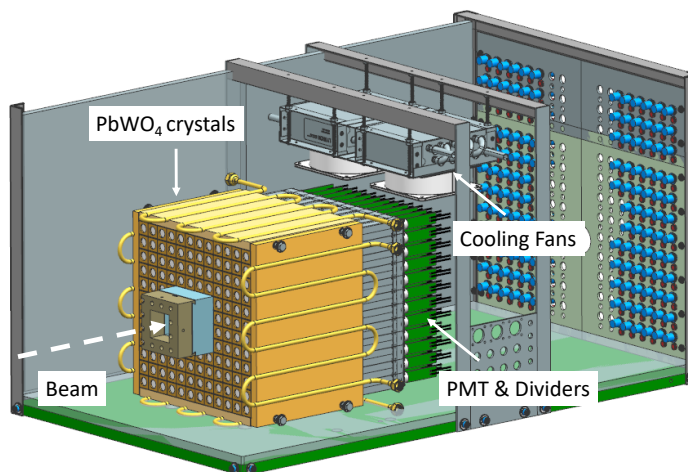


Figure 2: Schematic layout of the Compton calorimeter.

68 of the solenoid magnet was switched off in order to allow reconstruction of Compton
 69 events. The photon flux was about $5 \cdot 10^6 \gamma/\text{sec}$ (about five times lower than the nominal
 70 GlueX flux) in the beam energy range of interest between 9.5 GeV and 11.6 GeV.

71 **3. Compton calorimeter of the PrimEx- η experiment**

72 *3.1. Calorimeter design*

73 The calorimeter design is shown in Fig. 2. The CCAL comprises an array of 12×12
 74 lead tungstate modules with a 2×2 hole in the middle for the passage of the photon
 75 beam. The modules are positioned inside a light tight box. A tungsten absorber is
 76 placed in front of the innermost layer closest to the beamline to provide protection from
 77 the high rate of particles predominantly originating from electromagnetic interactions.

78 The light yield from PbWO_4 crystals depends on temperature with a typical coef-
 79 ficient of $2\%/^\circ\text{C}$ at room temperature. Maintaining constant temperature is essential
 80 for the calorimeter operation. The calorimeter modules are surrounded by four copper
 81 plates with built-in pipes to circulate a cooling liquid and provide temperature stabi-
 82 lization. Foam insulation surrounds the detector box. The temperature was monitored

83 and recorded during the experiment by five thermocouples attached to different points
84 of the PbWO_4 module assembly. During the experiment the temperature was main-
85 tained at $17^\circ \pm 0.2^\circ\text{C}$. The typical heat released by the photomultiplier tube (PMT)
86 dividers of the whole detector was equivalent to about 30 Watts. In order to prevent
87 condensation, a nitrogen purge was applied. Two fans with a water-based cooling sys-
88 tem were installed on the top of the crystal assembly to improve nitrogen circulation
89 and heat dissipation from the PMT dividers. The detector was positioned on a platform,
90 which allowed to move it in the vertical and horizontal directions, perpendicular to the
91 beam. The platform was remotely controlled and provided a position accuracy of about
92 $200\ \mu\text{m}$. During detector calibration each module was moved into the beam.

93 *3.2. Module design*

94 The design of the PbWO_4 module is based on the HyCal calorimeter, which was
95 used in several experiments in Jefferson Lab Hall B [13, 14]. An assembled calorime-
96 ter module is presented in Fig. 3. Each lead tungstate crystal is wrapped with a $60\ \mu\text{m}$
97 polymer Enhanced Specular Reflector film (ESR) manufactured by 3MTM, which al-
98 lows 98.5% reflectivity across the visible spectrum. In order to improve optical isola-
99 tion of each module from its neighbors, each crystal is wrapped with a layer of $25\ \mu\text{m}$
100 thick Tedlar. The PMT is located inside a G-10 fiberglass housing at the rear end of the
101 crystal. Two flanges are positioned at the crystal and housing ends and are connected
102 together using $25\ \mu\text{m}$ brass straps, which are brazed to the sides of the flanges. Four
103 set screws are pressed to the PMT housing flange to generate tension in the straps and
104 hold the assembly together. Light from the crystal is detected using a ten-stage Hama-
105 matsu PMT 4125, which is inserted into the housing and is coupled to the crystal using
106 optical grease (EJ-550). The PMT diameter is 19 mm. The PMT is pushed towards the
107 crystal by using a G-10 retaining plate attached to the back of the PMT and four tension
108 screws applied to the PMT flange. The PMT is instrumented with a high-voltage (HV)
109 divider and amplifier positioned on the same printed circuit board attached to the PMT
110 socket.

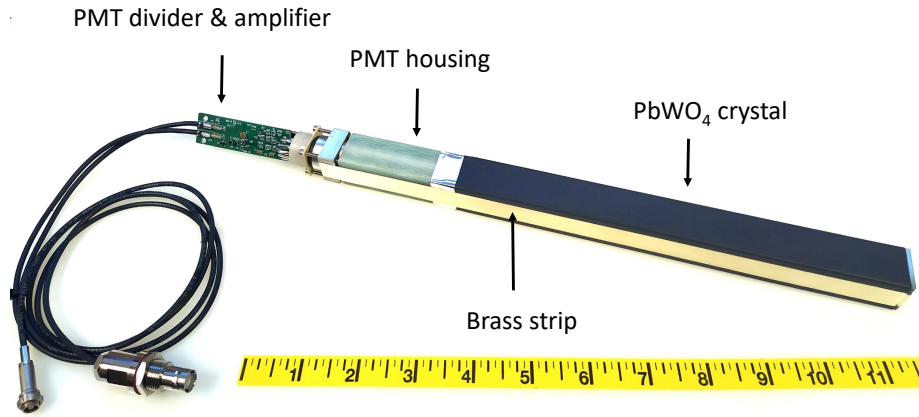


Figure 3: Calorimeter module showing main components: the PbWO_4 crystal, PMT housing, PMT divider, and signal and high-voltage cables.

111 3.3. Electronics

112 The PMT of each calorimeter module was equipped with an active base proto-
 113 type [15], which was designed for the Neutral Particle Spectrometer in experimen-
 114 tal Hall C. The base combines a voltage divider and an amplifier powered by the current
 115 flowing through the divider. The active base allows the operation of the PMT at lower
 116 voltage and consequently at lower anode current, which improves the detector rate ca-
 117 pability and prolongs the PMT's life. The original Hamamatsu divider for this type of
 118 PMT was modified by adding two bipolar transistors on the last two dynodes, which
 119 provides gain stabilization at high rate. The active base has a relatively large amplifica-
 120 tion of about a factor of 24 due to the large PMT count rate predicted by Monte Carlo
 121 simulation of the NPS detector. Large amplification was not needed for the planned
 122 run conditions of the PrimEx- η experiment. However, we subsequently used CCAL
 123 in GlueX runs at significantly larger luminosity in order to study run conditions of the
 124 FCAL lead tungstate insert, where the amplifier will be required. This will be dis-
 125 cussed in Section 4.0.3. During the PrimEx run, the CCAL PMTs were operated at
 126 about 680 V, which produced a divider current of 260 μA . The high voltage for each

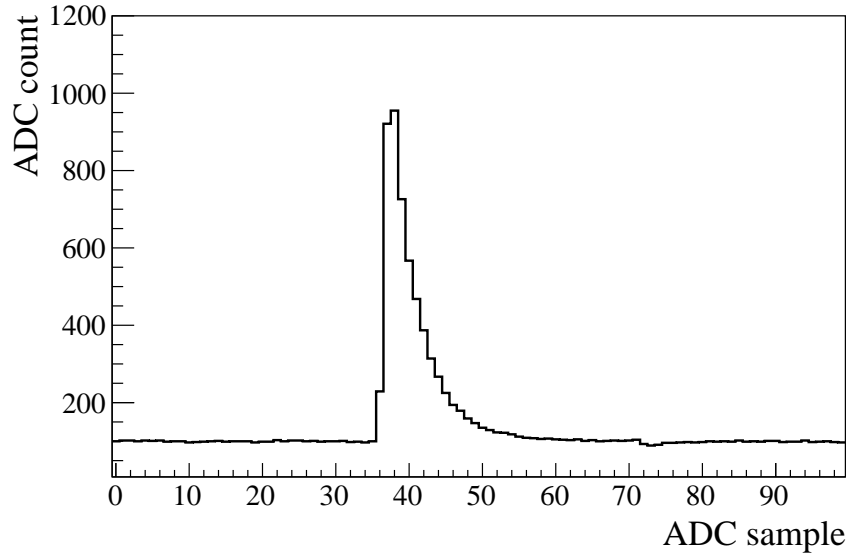


Figure 4: A typical flash ADC signal pulse obtained from a PbWO₄ module.

127 PMT was supplied by a 24-channel CAEN A7236SN module positioned in a SY4527
 128 mainframe.

129 Amplified PMT signals were digitized using a twelve-bit 16-channel flash ADCs
 130 electronics module operated at a sampling rate of 250 MHz. The ADC was designed
 131 at Jefferson Lab [16] and is used for the readout of several sub-detectors of the GlueX
 132 detector. The Field-Programmable Gate Array (FPGA) chip inside the ADC module
 133 allows the implementation of various programmable data processing algorithms for the
 134 trigger and readout. An example of a flash ADC signal pulse obtained from a calorime-
 135 ter module is shown in Fig. 4. In this example, the ADC is operated in the raw readout
 136 mode, where digitized amplitudes are read out for 100 samples, corresponding to the
 137 read out window size of 400 ns. During the PrimEx- η experiment, the ADC performed
 138 on-board integration of signal pulses, which amplitudes were above a threshold of 24
 139 MeV. Amplitudes were summed in a time window of 64 ns and read out from the ADC
 140 module along with other parameters such as the pulse peak amplitude, pulse time, and
 141 data processing quality factors. This readout mode allowed to significantly reduce the

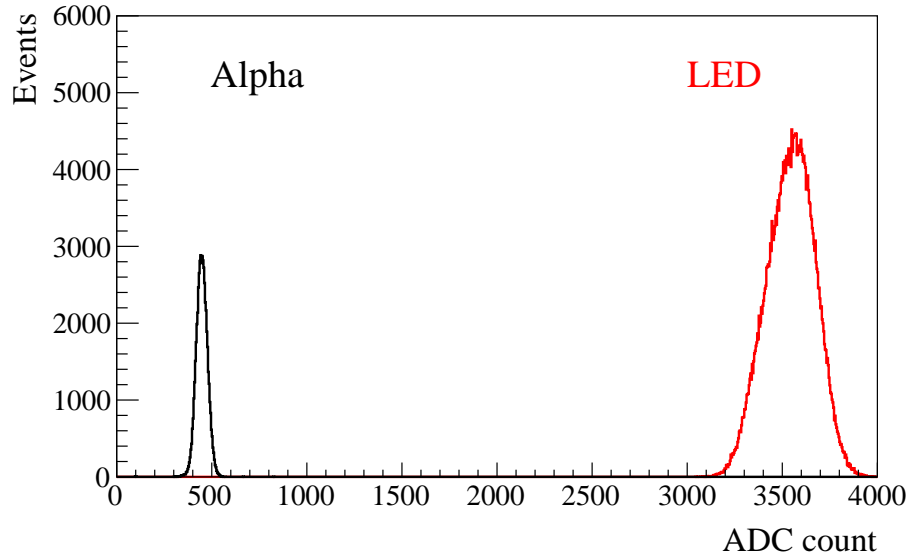


Figure 5: Flash ADC signal amplitudes induced by the LED and α -source in the reference PMT.

142 data size and ADC readout time, and therefore did not induce any dead time in the data
 143 acquisition.

144 CCAL flash ADCs are positioned in a VXS (ANSI/VITA 41.0 standard) crate. VXS
 145 crates are used to host all readout electronics of the GlueX experiment. In addition to
 146 the VME-bus used to read out data from electronics modules, the VXS is instrumented
 147 with a high-speed serial bus in order to increase the bandwidth to several Gb/sec and
 148 provide an interconnected network between modules. The bus is used to transmit am-
 149 plitudes digitized by the ADC to trigger electronics modules to include the CCAL in
 150 the Level 1 trigger system of the GlueX detector.

151 3.4. Light Monitoring System

152 To monitor performance of each calorimeter channel, we designed an LED-based
 153 light monitoring system (LMS). The LMS optics includes a blue LED, a spherical lens
 154 to correct the conical dispersion of the LED, and a diffusion grating to homogeneously
 155 mix the light. Light produced by the LED is incident on a bundle of plastic optical
 156 fibers (Edmund Optics) with a core diameter of 250 μm . Each fiber distributes light

157 to an individual calorimeter module. On the crystal end, the fiber is attached to the
158 module using a small acrylic cap glued to the crystal with a hole drilled through each
159 cap to hold the fiber inside.

160 To monitor stability of the LED, we used two reference Hamamatsu 4125 PMTs,
161 the same type as in the CCAL detector. Each PMT receives light from two sources: a
162 single fiber from the LED and a YAP:Ce pulser unit, both glued to the PMT face. The
163 pulser unit consists of a 0.15 mm thick YAP:Ce scintillation crystal with a diameter of
164 3 mm spot activated by an ^{241}Am α source. The α source is used to monitor stability of
165 the LED. The PMT was read out using a flash ADC. The high voltage on each reference
166 PMT was adjusted to have the signals from both the LED and α source fit within the
167 range of a 12-bit flash ADC corresponding to 4096 counts, as shown in Fig. 5. Each
168 LED was driven by a CAEN 1495 module, which allowed to generate LED pulses
169 with a programmable rate. The LMS was integrated into the GlueX trigger system
170 and provided a special trigger type during data taking. The LMS was extensively used
171 during the detector commissioning and injected light to the CCAL detector with a
172 typical frequency of 100 Hz continuously during the PrimEx- η experiment. This LED
173 rate is similar to the trigger rate of events produced by the reference α source.

174 Most LMS components were positioned inside the temperature-stabilized detector
175 box. The stability of the LED system measured using the reference PMTs during the
176 entire PrimEx run was on the level of 1%. The ratio of signal ADC amplitudes from
177 the LED pulser to the α source obtained during different run periods of the 48-day
178 long PrimEx- η experiment is presented in Fig. 6. The ratio is normalized to the data
179 in the beginning of the experiment. Stability of most CCAL modules observed using
180 the LMS during the experiment was better than 6%. We did not apply any PMT gain
181 adjustments during the experiment.

182 3.5. Calibration

183 The initial energy calibration of the CCAL was performed by moving the calorime-
184 ter platform and positioning each module into the photon beam during special low-
185 intensity calibration runs. The maximum rate in the module exposed to the beam did
186 not exceed 200 kHz at a threshold of 15 MeV. The energy of each beam photon was

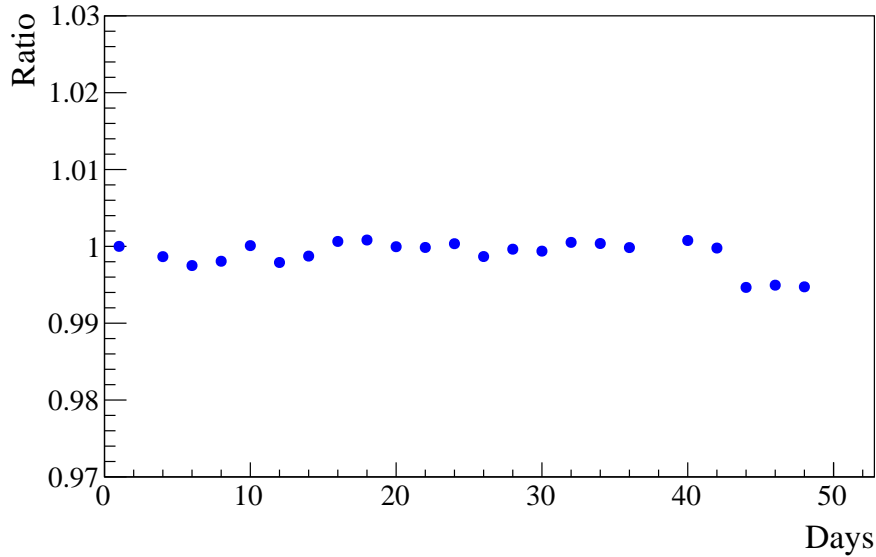


Figure 6: Ratio of signal ADC amplitudes from the LED pulser to the α -source measured by the reference PMT during different run periods of the 48-day long PrimEx- η experiment. The ratio is normalized to data in the beginning of the run.

187 determined by detecting a bremsstrahlung electron using the GlueX tagging detectors
 188 described in Section 2. The spot size of the collimated photon beam had a diameter of
 189 about 6 mm.

190 In the beginning of the calibration run, we adjusted the PMT high voltage for each
 191 module in order to equalize signal pulse amplitudes induced by 11 GeV beam photons.
 192 The amplitude was set to 3500 ADC counts, which corresponds to ~ 1.7 V. An ex-
 193 ample of flash ADC signal amplitude in the calorimeter module as a function of the
 194 beam energy is presented in Fig. 7. The calibration of each module was refined by
 195 reconstructing showers in the calorimeter and constraining the reconstructed energy to
 196 the known beam energy.

197 During the calibration runs, we estimated the non-uniformity of the 140 CCAL
 198 modules by measuring the relative energy resolution for each individual module ex-
 199 posed to the beam. The energy resolution obtained for 6 GeV photons is presented
 200 in Fig. 8. The distribution is fit to a Gaussian function. The non-uniformity of the

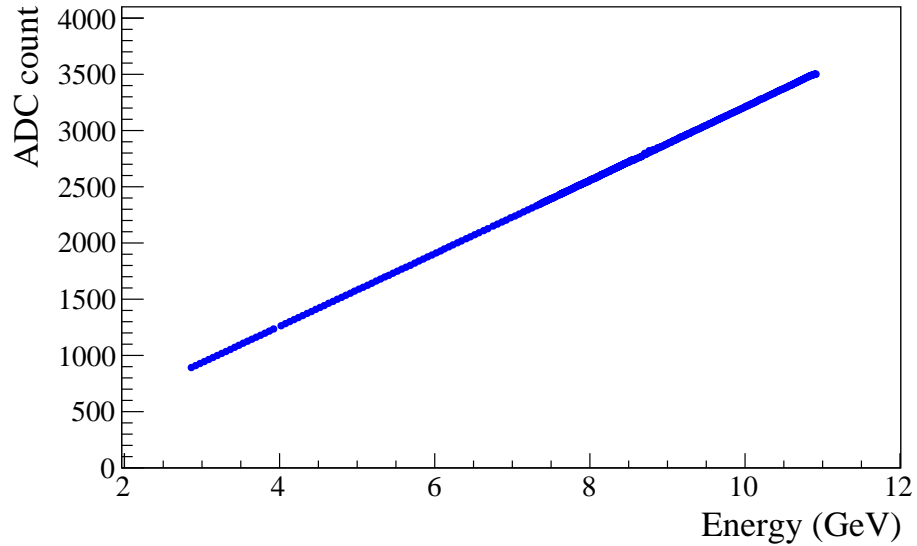


Figure 7: ADC signal pulse amplitude in the CCAL module as a function of the beam energy.

201 modules, i.e., the spread of the distribution is found to be smaller than 5%.

202 During calibration, we observed some non-linearity of the PMT active base with the
 203 large amplification factor of 24, on the level of a few percent, which impacted both the
 204 pulse peak and pulse integral. The base performance became linear when the amplifier
 205 gain was reduced. In order to study the impact of the non-linearity on the detector
 206 energy resolution, we replaced the original PMT active bases for 9 CCAL modules (in
 207 the array of 3×3 modules) with modified bases where the amplifier was bypassed.
 208 After adjusting high voltages and recalibrating PMT gains, we measured the energy
 209 resolution for different beam energies. The beam was incident on the center of the
 210 middle module in the array. An example of the energy deposited by 10 GeV photons is
 211 shown in Fig. 9. The energy resolution was obtained from a fit of the energy distribution
 212 to a Crystal Ball function³ implemented in the ROOT data analysis framework [17].
 213 The energy resolution as a function of the beam energy is shown in Fig. 10. The

³The function is named after the Crystal Ball collaboration.

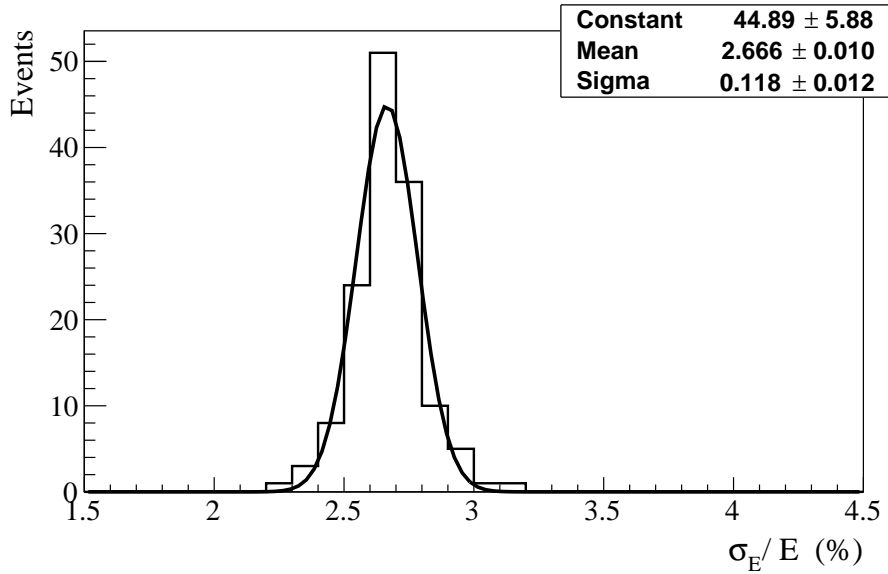


Figure 8: Relative energy resolution of 140 PbWO₄ modules installed on the CCAL measured with 6 GeV beam photons.

214 distribution was fit to the following function:

$$\frac{\sigma_E}{E} = \frac{S}{\sqrt{E}} \oplus \frac{N}{E} \oplus C, \quad (1)$$

215 where S represents the stochastic term, N the electronic noise and C the constant term,
 216 E is the beam energy in GeV, and the symbol \oplus indicates a quadratic sum. The fit
 217 yields: $S = 2.63 \pm 0.01\%$, $N = 1.07 \pm 0.09\%$, and $C = 0.53 \pm 0.01\%$. The resolution
 218 was found to be about 10% better than that measured with the original base with the
 219 amplifier gain of 24⁴. The energy resolution is consistent with that of the HyCal
 220 calorimeter [13], which was instrumented with crystals produced by SICCAS in 2001
 221 and was used in several experiments in Jefferson Lab's experimental Hall B. The HyCal
 222 PbWO₄ crystals have the same transverse size of 2.05 cm × 2.05 cm, but a smaller
 223 length of 18 cm. The initial CCAL calibration performed with the beam scan was fine-

⁴The linearity of the PMT active base is being currently improved; modified active bases will be installed before the new PrimEx- η run in 2021.

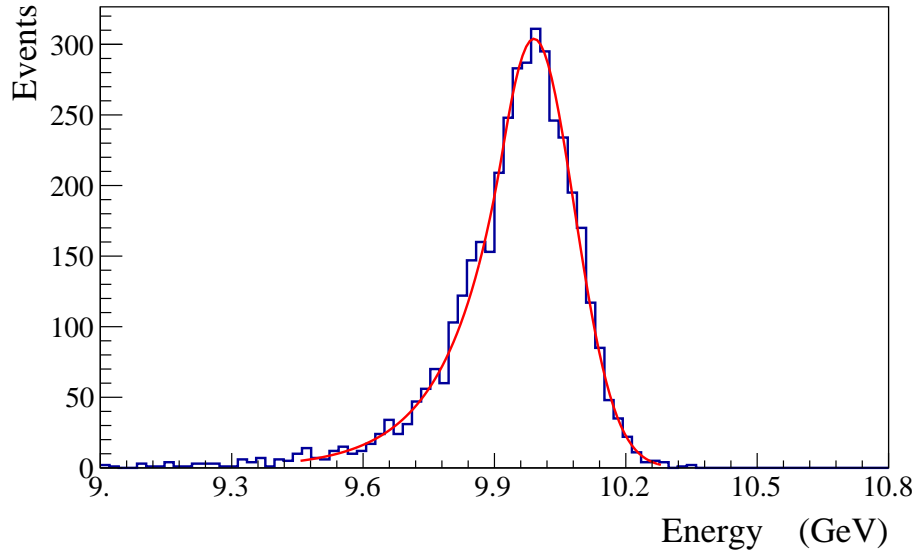


Figure 9: Energy distribution deposited by 10 GeV beam photons. The spectrum is fit to a Crystal Ball function.

224 tuned after the PrimEx- η run by using showers of reconstructed Compton scattering
 225 candidates and constraining the reconstructed energy in the event to the know beam
 226 energy.

227 3.6. Performance during the PrimEx- η run

228 In the PrimEx- η experiment, we reconstruct Compton events produced by beam
 229 photons with the energy larger than 6 GeV. This energy range is covered by the GlueX
 230 pair spectrometer [18], which determines the photon flux needed for cross section
 231 measurements. An electron and photon produced in the Compton scattering process
 232 were detected by reconstructing two showers, one in the FCAL and another one in
 233 the CCAL. The event topology of the reaction is such that the more energetic electron
 234 predominantly goes into the Compton calorimeter, while the photon strikes the FCAL.
 235 In order to accept Compton events during data taking and to reduce background orig-
 236 inating from low-energy electromagnetic and hadronic interactions, the CCAL was
 237 integrated to the Level 1 trigger system of the GlueX detector. The physics trigger was

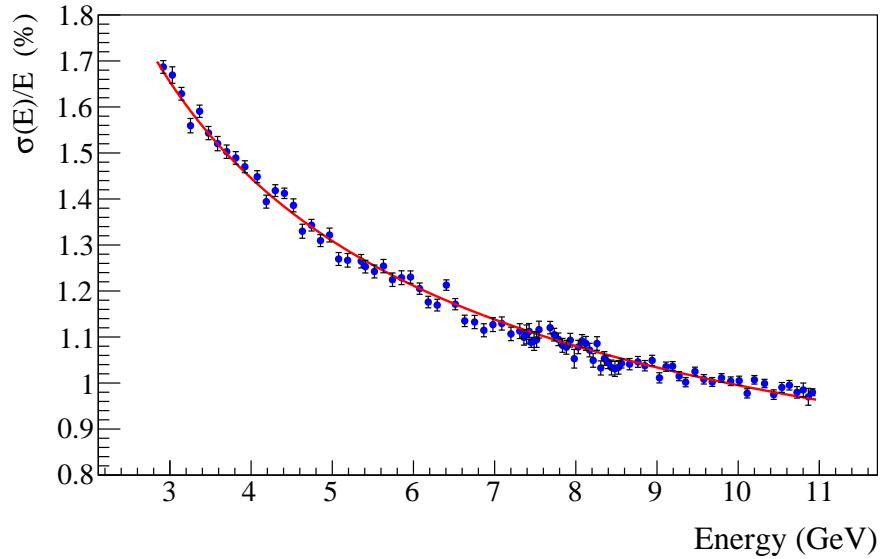


Figure 10: The CCAL energy resolution as a function of the photon energy.

238 based on the total energy deposited in the forward and Compton calorimeters. The
 239 GlueX trigger is implemented on special-purpose programmable electronics modules
 240 with FPGA chips. The trigger architecture is described in Ref. [19]. The trigger rate
 241 as a function of the energy threshold is presented in Fig. 11. We collected data using a
 242 relatively small energy threshold of 3 GeV at a trigger rate of about 18 kHz. This rate
 243 did not produce any dead time in the data acquisition and trigger systems. The trigger
 244 rate was reproduced by a detailed Geant detector simulation.

245 The rate in the CCAL modules during the experiment is presented in Fig. 12. In
 246 this plot, the photon beam goes through the center of the hole of 2×2 modules in the
 247 middle of the detector. The rate is the largest in innermost detector layers closest to
 248 the beamline. The maximum rate in the detector module was about 200 kHz for an
 249 energy threshold of 30 MeV, which is equivalent to a signal pulse amplitude of 5 mV.
 250 Before the experiment, we performed a high-rate performance study of the PMT and
 251 electronics using a laser and an LED pulser and did not find any degradation of the
 252 PMT gain up to 2 MHz [20].

253 Timing resolution of reconstructed showers is an important characteristic of the
254 detector performance. In the experiment we used timing information provided by the
255 calorimeters to identify the accelerator beam bunch for which the interaction occurred
256 in the detector and therefore relate showers in the calorimeters with hits in the tagging
257 detector, from the same event. A hit in the tagging detector defines the energy of the
258 beam photon. The time in the calorimeter module is provided by an algorithm imple-
259 mented on the programmable FPGA chip of the flash ADC. The algorithm performs a
260 search of the peak of the signal pulse and determines the time from the shape of the
261 leading edge of the pulse. The times of all hits constituting the CCAL shower are com-
262 bined to form the shower time by using an energy-weighted sum. The time difference
263 between beam photon candidates and CCAL showers originating from Compton events
264 is presented in Fig. 13. The main peak on this plot corresponds to beam photons and
265 CCAL clusters produced in the same accelerator bunch. Satellite peaks, separated by
266 the beam bunch period of about 4 ns, represent accidental beam photons from acceler-
267 ator bunches not associated with the interaction in the detector. The time resolution of
268 CCAL showers is improved with the increase of the shower energy and was measured
269 to be about 330 ps and 140 ps for 1 GeV and 9 GeV showers, respectively. In the
270 PrimEx- η experiment the CCAL allowed a clear separation of beam photons originat-
271 ing from different beam bunches.

272 Reconstruction of electromagnetic showers in the FCAL is performed using an
273 algorithm described in Ref. [21], which is a part of the standard GlueX reconstruction
274 software. For the CCAL, we implemented an algorithm originally developed for the
275 GAMS spectrometer [22, 23], which was subsequently adopted for the HyCal [13] in
276 JLab's experimental Hall B. The algorithm provides a good separation of overlapping
277 showers in the calorimeter by using profiles of electromagnetic showers. The elasticity
278 distribution, defined as the reconstructed energy in the event minus the beam energy, is
279 presented in Fig. 14 for Compton candidates produced by beam photons in the energy
280 range between 6 GeV and 7 GeV. The solid line shows the fit of this distribution to the
281 sum of a Gaussian and a second order polynomial function. The energy resolution of
282 reconstructed Compton candidates in this energy range is about 130 MeV. In this plot,
283 we subtracted background originating from accidental beam photons. This background

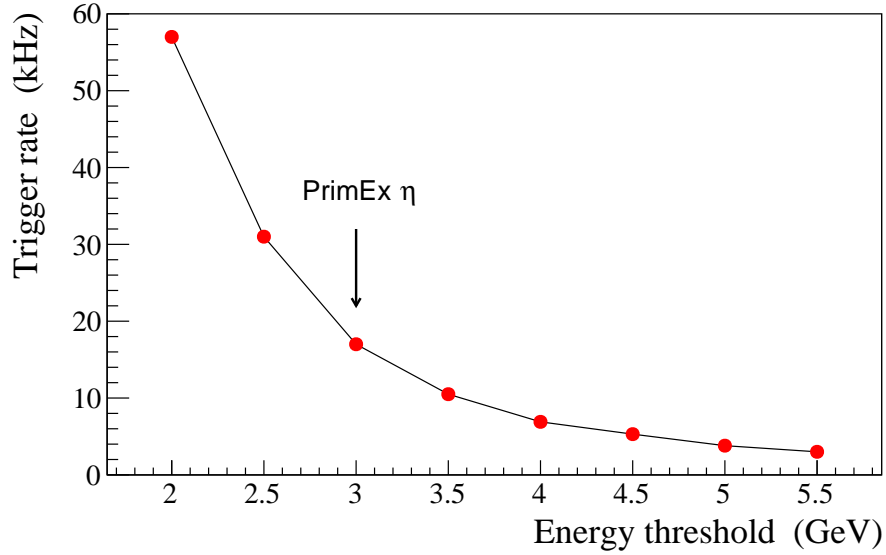


Figure 11: Trigger rate as a function of the total energy deposited in the FCAL and CCAL. The arrow indicates the energy threshold used in PrimEx- η production runs.

284 was measured using off-time interactions and amounted to about 15%. The relatively
 285 small background, on the level of 10%, produced by interactions of the photon beam
 286 with the beamline material downstream the GlueX target was measured using empty-
 287 target runs and was also excluded from the elasticity distribution in Fig. 14. The CCAL
 288 allowed to clearly reconstruct Compton events in the PrimEx- η experiment.

289 4. Upgrade of the GlueX forward calorimeter

290 The forward calorimeter of the GlueX detector consists of 2800 lead glass modules,
 291 each with a size of 4 cm \times 4 cm \times 45 cm, and is positioned about 6 m downstream
 292 of the target, as shown in Fig. 1. The FCAL covers a polar angle of photons produced
 293 from the target between 1° and 11° and detects showers with energies in the range of
 294 0.1 - 8 GeV. The Cherenkov light produced in the module is detected by FEU-84-3
 295 photomultiplier tubes, instrumented with Cockcroft-Walton bases [24]. The typical
 296 energy resolution of the FCAL is $\sigma_E/E = 6.2\%/\sqrt{E} \oplus 4.7\%$ [1].

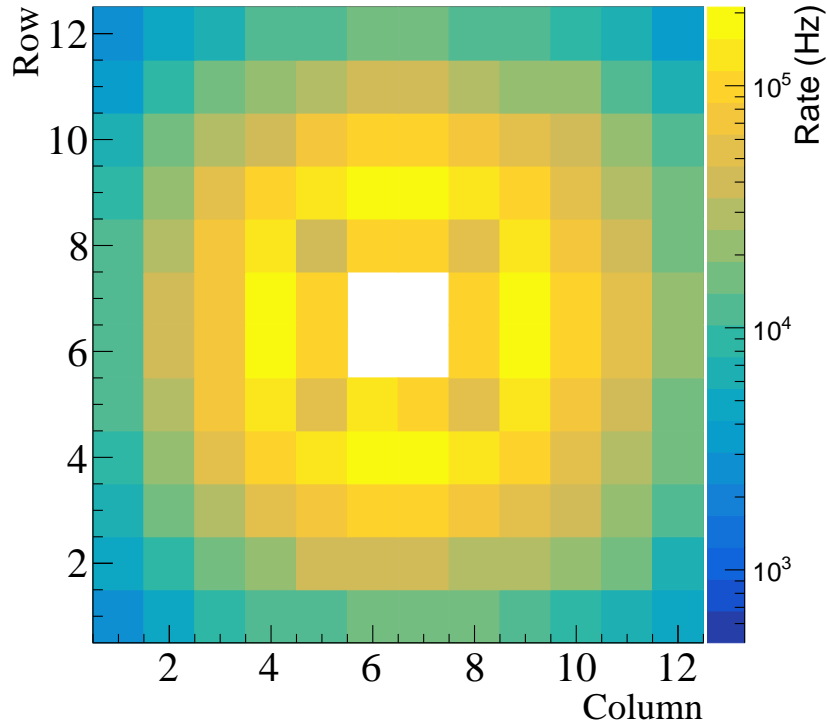


Figure 12: Rates in the CCAL modules during PrimEx- η production run. The energy threshold corresponds to 30 MeV. The beam goes through the center of the hole in the middle of the plot.

297 The future physics program with the GlueX detector in Hall D will require an up-
 298 grade of the inner part of the forward calorimeter with high-granularity, high-resolution
 299 PbWO_4 crystals. The lead tungstate insert will improve the separation of clusters in the
 300 forward direction and the energy resolution of reconstructed photons by about a fac-
 301 tor of two. Lead tungstate crystals possess better radiation hardness compared to lead
 302 glass, which is important for the long term operation of the detector at high luminosity.
 303 The size of the insert will tentatively comprise 1596 PbWO_4 crystals, which will form
 304 an array of 40×40 modules ⁵. Similar to the CCAL, the insert will have a beam hole

⁵The insert size proposed for the JEF experiment [2] is $1 \text{ m} \times 1 \text{ m}$; the actual size will depend on the

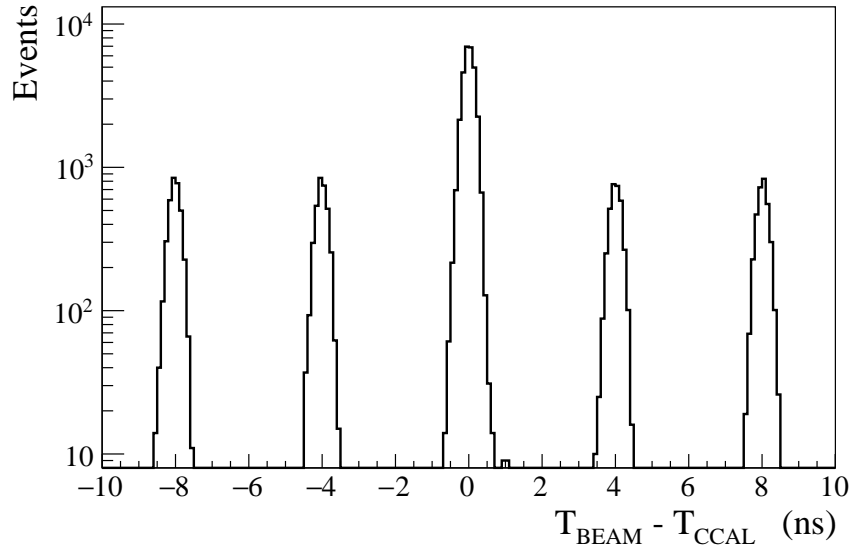


Figure 13: Time difference between beam photons and reconstructed CCAL showers for Compton candidates. Peaks are separated by the beam bunch period of 4 ns.

305 of 2×2 modules and a tungsten absorber used to shield the detector layer closest to
 306 the beamline. A schematic view of the FCAL frame with the installed lead tungstate
 307 insert is presented in Fig. 15. Due to the different size of the lead glass bars and lead
 308 tungstate crystals, the lead glass modules stacked around the PbWO_4 insert will form
 309 four regions with a relative offset between modules; those regions are shown in green
 310 color in this plot.

311 The PbWO_4 module design of the FCAL insert will essentially be the same as for
 312 the CCAL, except for some small modifications needed to handle the magnetic field
 313 present in the FCAL region. The PMT housing made of the G-10 fiberglass material
 314 will be replaced by iron housing in order to reduce the magnetic field. The housing
 315 length will be increased to extend the magnetic shield beyond the PMT photocathode.
 316 An acrylic optical light guide will be inserted inside the PMT housing to couple the
 317 crystal and PMT.

availability of funds.

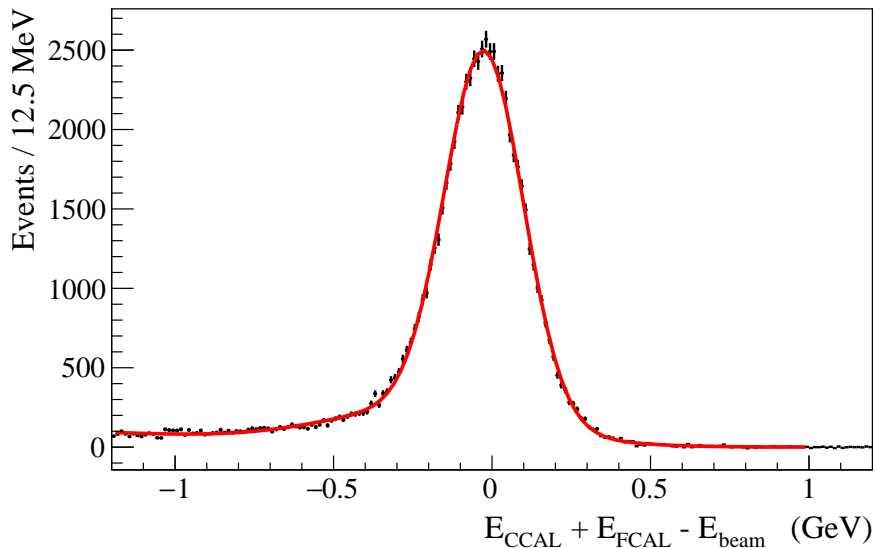


Figure 14: Elasticity distribution of reconstructed Compton candidates.

318 The upgraded FCAL will be operated in GlueX experiments using a 30 cm long
 319 liquid hydrogen target at the designed photon flux of $5 \cdot 10^7 \gamma/\text{sec}$ in the energy range
 320 between 8.4 GeV and 9 GeV. The designed luminosity is significantly larger than that
 321 used in the PrimEx- η experiment and was achieved after the PrimEx run in the fall
 322 of 2019. In order to finalize the design of the PMT electronics, it is important to
 323 understand detector rates in the FCAL insert, especially in layers close to the beamline.
 324 We used the CCAL during high-intensity GlueX runs to study run conditions for the
 325 FCAL insert.

326 4.0.1. Magnetic shielding of PMTs

327 The longitudinal (directed along the beamline) and transverse (directed perpendic-
 328 ular to the axis of the beamline) components of the magnetic field produced by the
 329 GlueX solenoid magnet in the FCAL PbWO_4 insert area vary between 40 - 55 Gauss
 330 and 0 - 9 Gauss, respectively. The longitudinal field is the largest on the beamline,
 331 where the transverse component is practically absent. We studied the PMT magnetic
 332 shielding using a prototype consisting of an array of 3×3 PMT iron housings made of

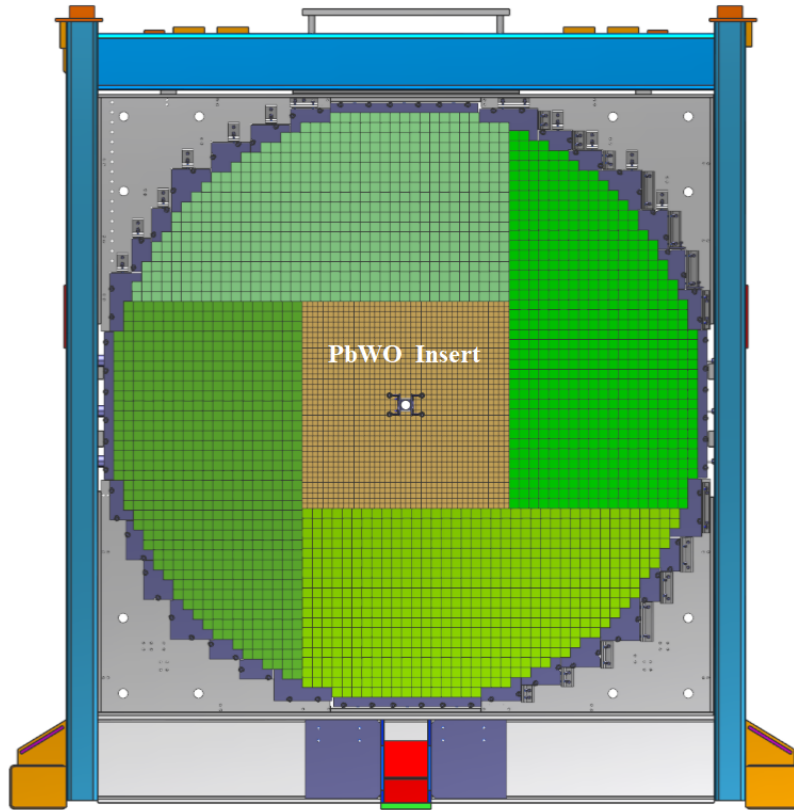


Figure 15: FCAL frame with calorimeter modules installed: PbWO_4 crystals (brown area), lead glass blocks (green). The photon beam passes through the hole in the middle of the calorimeter.

333 AISI 1020 steel, which was positioned in the middle of Helmholtz coils. Each housing
 334 had a size of $20.6 \text{ mm} \times 20.6 \text{ mm} \times 104 \text{ mm}$ with a 20 mm round hole in the middle
 335 for the PMT. This corresponds to the realistic size of the magnetic shield that will be
 336 used in the calorimeter module assembly. Inside the housing we inserted two layers of
 337 mu-metal cylinders, with thicknesses of $350 \mu\text{m}$ and $50 \mu\text{m}$, separated from each other
 338 by a Kapton film. The thickest cylinder was spot welded and annealed.

339 The Helmholtz coils had a diameter of about 1.5 m and can generate a uniform
 340 magnetic field with variable strength below 100 Gauss. A Hall probe was inserted
 341 into the central module of the prototype to measure the magnetic field at different Z-

342 positions along the length of the cylinder. The field was measured for two different
343 orientations of the prototype with respect to the magnetic field: field oriented along the
344 PMT (longitudinal, B_z) and perpendicular to the PMT housing (transverse, B_x). Field
345 measurements are presented in Fig. 16. The PMT shield significantly reduces both the
346 longitudinal and transverse fields to the level of $B_z \sim 1$ Gauss and $B_x \ll 1$ Gauss. The
347 transverse field, which is well shielded, is more critical for the PMT operation, as it
348 is directed perpendicular to the electron trajectory inside the photo tube and deflects
349 electrons, resulting in the degradation of the photon detector efficiency and gain. The
350 field reaches a plateau at $Z = 3$ cm from the face of the housing. We will use 3.5 cm
351 long acrylic light guides, in order to place the most sensitive to the magnetic field area
352 of the PMT between the photocathode and the last dynode (4.6 cm long) in the region
353 with the smallest magnetic field, as shown in Fig. 16. The actual field inside the FCAL
354 insert module is expected to be even smaller due to the collective shielding effect, i.e.,
355 the large amount of shielding material installed on surrounding modules [25].

356 We studied performance of the shielded PMT in the magnetic field using an LED
357 pulser. A blue LED with a light diffuser was placed about 20 cm from the PMT housing
358 prototype and was aligned with the middle module. The PMT response was measured
359 for different pulse amplitudes and operational high voltages. In order to study the con-
360 tributions from longitudinal and transverse field components we rotated the prototype
361 by different angles. Signal amplitudes as a function of the magnetic field measured in
362 the prototype tilted by about 10 degrees are presented on the top plot of Fig. 17. Am-
363 plitudes, normalized to measurements without magnetic field, are shown on the bottom
364 plot. The relative degradation of the signal amplitude for the maximum field in the
365 FCAL insert region of $B = 55$ Gauss ($B_z \sim 54$ Gauss and $B_x \sim 9$ Gauss) was measured
366 to be on the level of 1%. The proposed shielding configuration is sufficient to reduce
367 the magnetic field to the level suitable for the PMT operation.

368 4.0.2. Light guide studies

369 Studies of the magnetic shielding demonstrated that the PMT has to be positioned
370 inside the iron housing at the distance of at least 3 cm from the face of the PbWO_4
371 crystal. In order to do this, in the FCAL insert module we decided to use a 3.5 cm long

372 acrylic cylindrical light guide with a diameter of 18.5 mm between the PMT and the
373 PbWO_4 crystal. The light guide is wrapped with reflective ESR foil and attached to the
374 PMT with Dymax 3094 UV curing glue. Optical coupling to the crystal is provided
375 by a “silicon cookie”: a 1 mm thick transparent rubber cylinder made of the room
376 temperature vulcanized silicon compound, RTV615. The silicon cookie is not glued
377 to the light guide or the crystal, so the module can be easily disassembled if its PMT
378 needs to be replaced.

379 We compared light losses of the FCAL insert module instrumented with the light
380 guide with the CCAL module, where the PMT was coupled directly to the crystal using
381 an optical grease. Light collection was measured using electrons provided by the Hall
382 D pair spectrometer (PS) [18]. The PS is used to measure the flux of beam photons
383 delivered to the experimental hall by detecting electromagnetic electron-positron pairs
384 produced by the photons in a thin converter inserted to the beam. Leptons from the pair
385 are deflected in a dipole magnet and registered using scintillator detectors placed in the
386 electron and positron arms of the spectrometer. The energy of a lepton is detected using
387 a high-granularity PS hodoscope, which consists of 145 scintillating tiles and covers
388 the energy range between 3 GeV and 6 GeV. Each tile corresponds to the specific lepton
389 energy.

390 The relative light yield of the module with and without the light guide was estimated
391 by positioning the module behind the PS and measuring signal amplitudes induced by
392 the PS electrons. We first measured the ADC response in the CCAL module, which was
393 subsequently modified by adding the light guide to the same PMT and crystal and was
394 placed to the same spot of the PS test setup. Results of the measurements are presented
395 in Fig. 18. The ADC amplitude of the calorimeter module is presented as a function
396 of the PS tile for the two module configurations with and without the light guide. The
397 light guide results in a relatively small loss of light of 15 – 20% compared with the
398 CCAL module. We note that wrapping the light guide with the reflective material is
399 important. Losses in unwrapped light guide constitute about 35%. We repeated light
400 collection measurements using two more modules and obtained consistent results.

401 *4.0.3. Detector rate*

402 The PMT anode current is one of the critical characteristics that have to be consid-
403 ered during the design of the PMT divider. Typically the anode current should be on
404 the level of a few micro amperes and significantly smaller than the divider current in
405 order to provide stable performance of the PMT base and prevent the long-term degra-
406 dation of the PMT. Some lifetime tests of the Hamamatsu 4125 PMT are described in
407 Ref. [26].

408 The anode current (I) was measured in the CCAL modules during data production
409 runs at the GlueX nominal luminosity. It was obtained by measuring the average volt-
410 age in the flash ADC induced by particles incident on the CCAL module as follows:

$$I = \frac{\bar{U}}{R} \cdot \frac{1}{G}, \quad (2)$$

411 where \bar{U} is the average voltage in units of Volts, R is the input impedance of the am-
412 plifier ($\sim 50 \Omega$), and G is the amplifier gain of 24. A periodic pulser not associated
413 with an interaction in the detector was used as a trigger to read out flash ADC raw data
414 for each CCAL module in a time window of 400 ns. The voltage was determined by
415 summing up ADC amplitudes in the readout window and normalizing the sum to the
416 window size. The typical anode current measured in CCAL modules situated at differ-
417 ent distances from the beamline is presented in Fig. 19. Modules from the first CCAL
418 layer closest to the beamline and the outer most layer were not used in the analysis.
419 The inner modules were shielded by a tungsten absorber and the outer modules were
420 obscured by the FCAL. The rate in the detector is dominated by the forward-directed
421 electromagnetic background. The estimated anode current is the largest in the inner-
422 most layer of the detector closest to the beamline and amounts to about $1.4 \mu\text{A}$. This
423 current is significantly smaller than the PMT divider current of about $300 \mu\text{A}$.

424 We used the CCAL measurements to estimate the current in the FCAL insert. Tak-
425 ing the geometrical location of FCAL and CCAL modules into account, the largest
426 PMT current in the FCAL insert modules closest to the beamline and not shielded by
427 the absorber was conservatively estimated to be about $15 \mu\text{A}$. We assume that the PMT
428 base is operated at 1 kV and no amplifier is used. The detector rate drops rapidly with
429 the increase of the radial distance from the beamline. The estimated anode current is

430 relatively large and must be reduced by lowering the PMT high voltage. We are con-
431 sidering to instrument PMTs in a few inner FCAL insert layers with an amplifier with a
432 gain of 5 and to omit the amplifier on other modules. We are planning to perform more
433 beam tests of the FCAL insert active base using the CCAL in forthcoming GlueX runs
434 in 2021 - 2022.

435 5. Neutral Particle Spectrometer

436 The NPS is a new facility in Hall C that will allow access to precision measurements
437 of small cross sections of reactions with neutral final states. The NPS consists of an
438 electromagnetic calorimeter preceded by a sweeping magnet. As operated in Hall C, it
439 replaces one of the focusing spectrometers.

440 The NPS science program currently features six fully approved experiments. E12-
441 13-010 [4] and E12-06-114 [5] experiments will measure the Exclusive Deeply Virtual
442 Compton Scattering and π^0 cross sections to the highest Q^2 accessible at Jefferson Lab.
443 Both experiments will provide important information for understanding Generalized
444 Parton Distributions (GPDs). The E12-13-007 [6] experiment will study semi-inclusive
445 π^0 electroproduction process and seeks to validate the factorization framework that is
446 needed by the entire 12 GeV Jefferson Lab semi-inclusive deep-inelastic scattering pro-
447 gram. Measurements of Wide-Angle and Timelike Compton Scattering reactions will
448 be performed by the E12-14-003 [7] and E12-17-008 [8] experiments. These measure-
449 ments will allow to test universality of GPDs using high-energy photon beams. The
450 NPS will also be used in the E12-14-005 [9] experiment to study exclusive production
451 of π^0 at large momentum transfers in the process $\gamma p \rightarrow \pi^0 p$.

452 The NPS science program requires neutral particle detection over an angular range
453 between 6 and 57.3 degrees at distances of between 3 and 11 meters ⁶ from the exper-
454 imental target. The experiments will use a high-intensity beam of electrons with the
455 energies of 6.6, 8.8, and 11 GeV, and a typical luminosity of $\sim 10^{38} \text{ cm}^{-2}\text{s}^{-1}$ as well
456 as a secondary beam of photons incident on a liquid hydrogen target. A vertical-bend

⁶The minimum NPS angle at 3 m is 8.5 degrees; at 4 m it is 6 degrees.

457 sweeping magnet with integrated field strength of 0.3 Tm will be installed in front of
458 the spectrometer in order to suppress and eliminate background of charged particle
459 tracks originating from the target. The photon detection is the limiting factor of the ex-
460 periments. Exclusivity of the reaction is ensured by the missing mass technique and the
461 missing-mass resolution is dominated by the energy resolution of the calorimeter. The
462 calorimeter is anticipated to provide the spacial resolution of 2-3 mm and the energy
463 resolution of about $2.5\%/\sqrt{E}$. The NPS consists of 1080 PbWO₄ crystals that form
464 an array of 30 × 36 modules. Similarly to the FCAL insert in Hall D, the NPS will be
465 built from the crystals of the same size, and instrumented with the same type of PMTs
466 and readout electronics. The details of the mechanical assembly and commissioning
467 of the NPS are currently under development and will be described in a forthcoming
468 publication.

469 The radiation hardness and good optical quality of lead tungstate crystals are critical
470 for the NPS calorimeter. The NPS collaboration, in a synergistic effort with the EIC
471 eRD1 consortium, has characterized to date over 1200 PbWO₄ crystals produced by
472 CRYTUR and SICCAS from 2014 to the present. The results of these studies have
473 been published in Ref. [10]. CRYTUR crystal samples were found to have greater
474 overall uniformity in transmittance and light yield, and better radiation hardness. Of
475 the samples characterized by the NPS collaboration 140 SICCAS crystals have been
476 used in the CCAL detector.

477 **6. Summary**

478 We described the design and performance of the Compton calorimeter, which was
479 constructed using 140 lead tungstate PbWO₄ crystals recently produced by SICCAS.
480 The calorimeter was successfully used in the PrimEx- η experiment in spring of 2019
481 for reconstruction of Compton scattering events. The CCAL served as a prototype for
482 two large-scale electromagnetic calorimeters based on the PbWO₄ crystals: the lead
483 tungstate insert of the forward calorimeter of the GlueX detector and the neutral par-
484 ticle spectrometer. Experience gained during construction and operation of the CCAL
485 provided important information for finalizing the design of FCAL PbWO₄ modules and

486 PMT dividers and also served to further optimize the NPS calorimeter. We presented
487 the design of the FCAL lead tungstate insert and gave an overview of the NPS project.

488 **7. Acknowledgments**

489 This work was supported by the Department of Energy. Jefferson Science Asso-
490 ciates, LLC operated Thomas Jefferson National Accelerator Facility for the United
491 States Department of Energy under contract DE-AC05-06OR23177. This work was
492 supported in part by NSF grants PHY-1714133, PHY-2012430 and PHY-1812396, and
493 the U.S. Department of Energy Grant DE-FG02-03ER41231. We thank the NPS col-
494 laboration/project for providing PbWO_4 crystals and PMTs used in the construction of
495 the CCAL.

496 **References**

- 497 [1] S. Adhikari, et al., The GLUEX beamline and detector, Nucl. Instrum. Meth.
498 A 987 (2021) 164807. arXiv:2005.14272, doi:10.1016/j.nima.2020.
499 164807.
- 500 [2] JLab Experiment **E12-12-002**, Eta Decays with Emphasis on Rare Neutral
501 Modes: The JLab Eta Factory (JEF) Experiment, available online: [https://www.
502 jlab.org/exp_prog/proposals/14/PR12-14-004.pdf](https://www.jlab.org/exp_prog/proposals/14/PR12-14-004.pdf).
- 503 [3] T. Horn, et al., Scintillating crystals for the Neutral Particle Spectrometer in Hall
504 C at JLab, Nucl. Instrum. Meth. A 956 (2020) 163375. arXiv:1911.11577,
505 doi:10.1016/j.nima.2019.163375.
- 506 [4] JLab experiment **E12-13-010**, Exclusive Deeply Virtual Compton and Neutral
507 Pion Cross-Section Measurements in Hall C, available online: [https://www.
508 jlab.org/exp_prog/proposals/13/PR12-13-010.pdf](https://www.jlab.org/exp_prog/proposals/13/PR12-13-010.pdf).
- 509 [5] JLab experiment **E12-06-114**, Measurements of the Electron-Helicity Depen-
510 dent Cross Sections of Deeply Virtual Compton Scattering with CEBAF at 12
511 GeV, available online: [https://www.jlab.org/exp_prog/proposals/06/
512 PR12-06-114.pdf](https://www.jlab.org/exp_prog/proposals/06/PR12-06-114.pdf).

- 513 [6] JLab experiment **E12-13-007**, Measurement of SemiInclusive π^0 Production as
514 Validation of Factorization , available online: [https://www.jlab.org/exp_](https://www.jlab.org/exp_prog/proposals/13/PR12-13-007.pdf)
515 [prog/proposals/13/PR12-13-007.pdf](https://www.jlab.org/exp_prog/proposals/13/PR12-13-007.pdf).
- 516 [7] JLab experiment **E12-14-003**, Wide-angle Compton Scattering at 8 and 10
517 GeV Photon Energies, available online: [https://www.jlab.org/exp_prog/](https://www.jlab.org/exp_prog/proposals/14/PR12-14-003.pdf)
518 [proposals/14/PR12-14-003.pdf](https://www.jlab.org/exp_prog/proposals/14/PR12-14-003.pdf).
- 519 [8] JLab experiment **E12-17-008**, Polarization Observables in Wide-Angle Compton
520 Scattering at large s , t , and u , available online: [https://www.jlab.org/exp_](https://www.jlab.org/exp_prog/proposals/17/PR12-17-008.pdf)
521 [prog/proposals/17/PR12-17-008.pdf](https://www.jlab.org/exp_prog/proposals/17/PR12-17-008.pdf).
- 522 [9] JLab experiment **E12-14-005**, Wide Angle, Exclusive Photoproduction of π^0
523 Mesons, available online: [https://www.jlab.org/exp_prog/proposals/](https://www.jlab.org/exp_prog/proposals/14/PR12-14-005.pdf)
524 [14/PR12-14-005.pdf](https://www.jlab.org/exp_prog/proposals/14/PR12-14-005.pdf).
- 525 [10] T. Horn, et al., Scintillating crystals for the Neutral Particle Spectrometer in Hall
526 C at JLab, Nucl. Instrum. Meth. A 956 (2020) 163375. [arXiv:1911.11577](https://arxiv.org/abs/1911.11577),
527 [doi:10.1016/j.nima.2019.163375](https://doi.org/10.1016/j.nima.2019.163375).
- 528 [11] R. Abdul Khalek, et al., Science Requirements and Detector Concepts for the
529 Electron-Ion Collider: EIC Yellow Report [arXiv:2103.05419](https://arxiv.org/abs/2103.05419).
- 530 [12] JLab Experiment **E12-10-011**, A Precision Measurement of the η Radiative De-
531 cay Width via the Primakoff Effect, available online: [https://www.jlab.org/](https://www.jlab.org/exp_prog/proposals/10/PR12-10-011.pdf)
532 [exp_prog/proposals/10/PR12-10-011.pdf](https://www.jlab.org/exp_prog/proposals/10/PR12-10-011.pdf).
- 533 [13] M. Kubantsev, I. Larin, A. Gasparian, Performance of the PrimEx electromag-
534 netic calorimeter, AIP Conf. Proc. 867 (1) (2006) 51–58. [arXiv:physics/](https://arxiv.org/abs/physics/0609201)
535 [0609201](https://arxiv.org/abs/physics/0609201), [doi:10.1063/1.2396938](https://doi.org/10.1063/1.2396938).
- 536 [14] A. Gasparian, A high performance hybrid electromagnetic calorimeter at Jef-
537 ferson Lab, in: 11th International Conference on Calorimetry in High-Energy
538 Physics (Calor 2004), 2004.

- 539 [15] V. Popov, H. Mkrtchyan, New photomultiplier active base for hall c jefferson
540 lab lead tungstate calorimeter, in: 2012 IEEE Nuclear Science Symposium and
541 Medical Imaging Conference Record (NSS/MIC), 2012, pp. 1177–1179. doi :
542 10.1109/NSSMIC.2012.6551294.
- 543 [16] F. Barbosa, et al., A VME64x, 16-Channel, Pipelined 250 MSPS Flash ADC With
544 Switched Serial (VXS) Extension, Tech. rep., Jefferson Lab, Technical Report
545 GlueX-doc-1022 (hyperlink) (Apr. 2007).
- 546 [17] R. Brun, F. Rademakers, ROOT: An object oriented data analysis framework,
547 Nucl. Instrum. Meth. A 389 (1997) 81–86. doi:10.1016/S0168-9002(97)
548 00048-X.
- 549 [18] F. Barbosa, C. Hutton, A. Sitnikov, A. Somov, S. Somov, I. Tolstukhin, Pair spec-
550 trometer hodoscope for Hall D at Jefferson Lab, Nucl. Instrum. Meth. A 795
551 (2015) 376–380. doi:10.1016/j.nima.2015.06.012.
- 552 [19] A. Somov, Development of level-1 triggers for experiments at Jefferson Lab, AIP
553 Conf. Proc. 1560 (1) (2013) 700–702. doi:10.1063/1.4826876.
- 554 [20] F. Barbosa, et al., Characterization of the NPS and CCAL readout , Tech.
555 rep., Jefferson Lab, GlueX-doc-3272, (2017), [https://halldweb.jlab.org/
556 doc-public/DocDB/ShowDocument?docid=3272](https://halldweb.jlab.org/doc-public/DocDB/ShowDocument?docid=3272).
- 557 [21] R. T. Jones, et al., A bootstrap method for gain calibration and resolution determi-
558 nation of a lead-glass calorimeter, Nucl. Instrum. Meth. A 566 (2006) 366–374.
559 doi:10.1016/j.nima.2006.07.061.
- 560 [22] A. Lednev, Separation of the overlapping electromagnetic showers in the cellular
561 gams-type calorimeters., Tech. rep., IHEP Protvino, Preprint IHEP (1993) 93-
562 153.
- 563 [23] F. Binon, et al., Hodoscope multi-photon spectrometer GAMS-2000, Nucl. In-
564 strum. Meth. A 248 (1986) 86. doi:10.1016/0168-9002(86)90501-2.

- 565 [24] A. Brunner, et al., A Cockcroft-Walton base for the FEU84-3 photomulti-
566 plier tube, Nucl. Instrum. Meth. A 414 (1998) 466–476. doi:10.1016/
567 S0168-9002(98)00651-2.
- 568 [25] O. Glamazdin, TOSCA simulation of the magnetic shielding of the FCAL insert ,
569 Tech. rep., Jefferson Lab, GlueX-doc-3561, (2018), [https://halldweb.jlab.
570 org/doc-private/DocDB/ShowDocument?docid=3561](https://halldweb.jlab.org/doc-private/DocDB/ShowDocument?docid=3561).
- 571 [26] W. Koska, S. W. Delchamps, J. Freeman, W. Kinney, D. Lewis, P. Limon, J. Strait,
572 I. Fiori, M. Gallinaro, Q. Shen, Evaluation of candidate photomultiplier tubes for
573 the upgrade of the CDF end plug calorimeter, Nucl. Instrum. Meth. A 406 (1998)
574 103–116. doi:10.1016/S0168-9002(97)01193-5.

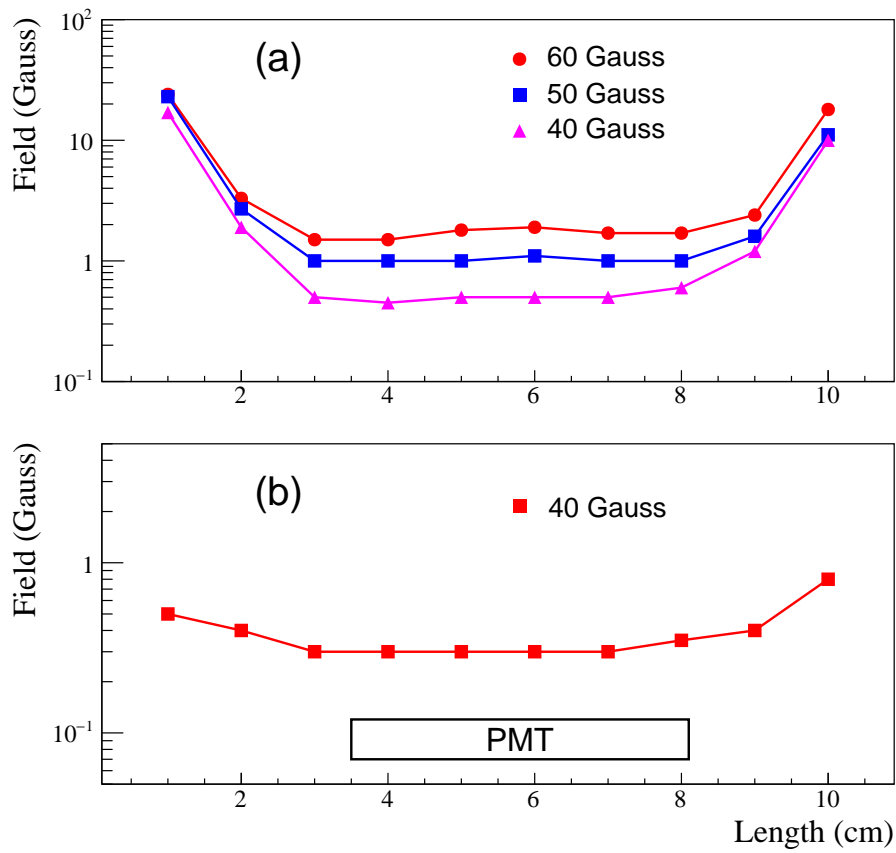


Figure 16: Magnetic field distribution inside the PMT shield housing as a function of the distance from the housing face. Plot (a) corresponds to the longitudinal field and plot (b) corresponds to the transverse field produced by the Helmholtz coils. Markers denote different field values.

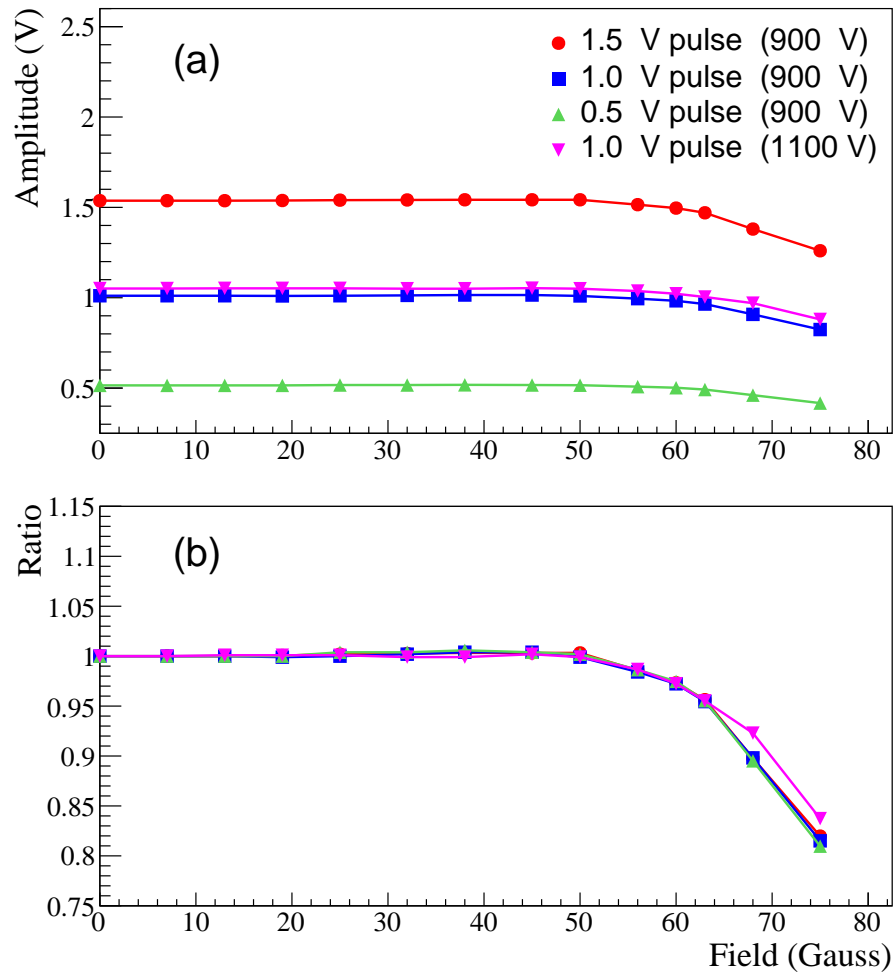


Figure 17: Signal amplitudes of shielded PMT induced by an LED as a function of the magnetic field (a). Amplitudes, normalized to measurements without magnetic field (b). The PMT response was measured for different intensities of light pulse and HV settings as shown by different polymarkers.

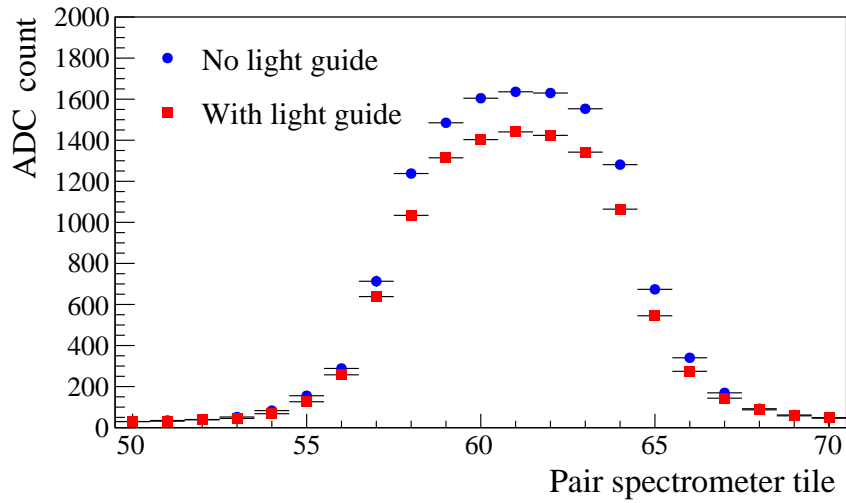


Figure 18: ADC amplitudes of the calorimeter module as a function of the pair spectrometer tile for two configurations: the PMT directly coupled to the PbWO₄ crystal (circles), and the PMT coupled to the module using optical light guide (boxes).

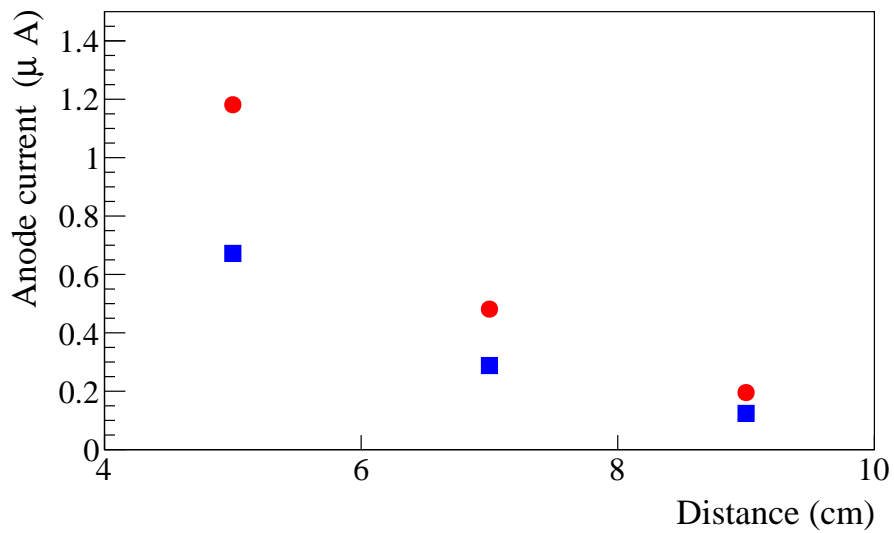


Figure 19: Typical PMT anode current of CCAL modules positioned at different distances from the beamline. Circles correspond to the nominal GlueX luminosity, boxes correspond to 60% of the nominal luminosity.